TIME-DEPENDENT FIBRE PULL-OUT BEHAVIOUR IN SELF-COMPACTING CONCRETE

Amin Abrishambaf *[1], Joaquim A. O. Barros[1], Vitor M.C.F. Cunha[1] and Cristina Frazão[1]

[1] ISISE, Dep. Civil Eng., School Eng., University of Minho, Campus de Azurém 4800-058 Guimarães, Portugal.

ABSTRACT

In the present study, the effectiveness of a fibre as an element for transferring stresses across cracks under a sustained load was assessed. Single fibre pull-out creep tests were performed, in which fibre slip was monitored as a function of the time. The influence of the fibre orientation angle (0, 30 and 60 degrees), as well as pre-imposed fibre slip levels, s_{pr}, 0.3 and 0.5 mm on the creep response was investigated. Additionally, instantaneous fibre pull-out tests were carried out on undamaged-bond specimens in order to quantify the effects of the pull-out creep behaviour. The damage introduced by the pre-slip levels in the bond of the fibre/matrix interface influenced the long-term fibre pull-out behaviour and, consequently, accelerated the creep rate. However, the assembled pull-out creep behaviour did not differ considerably from the instantaneous pull-out behaviour for the adopted pre-imposed fibre slip levels.

Keywords: Time-dependent behaviour; Long-term load; Creep; Fibre pull-out; Bond; Steel fibre reinforced self-compacting concrete.

* Author to whom the correspondence should be sent (amabrishambaf@gmail.com)
Tel: +351 253 510 210 Fax: +351 253 510 217

1. INTRODUCTION

The application of short and randomly distributed steel fibres is becoming increasingly more popular in concrete technology, since they can reduce the drawback deal with the concrete brittleness. In concrete reinforced with a relatively low fibre contents, the effectiveness of the fibre reinforcement becomes more predominant after cracking of the matrix, since fibres are the elements that transfer stress across the crack's surfaces. It is widely acknowledge that the mechanical behaviour of steel fibre reinforced concrete, SFRC, depends not only on the bond behaviour of the fibre/matrix interface, but also on how fibres are distributed and oriented throughout the matrix [1-4]. Consequently, considering that fibres and matrix are bonded by a weak interface, understanding this interfacial behaviour is of the utmost importance for a reliable predictive of the mechanical performance of such composites.

The creep deformation can compromise functionality of a structure due to abnormally high long-term deflection. The durability of cracked concrete structures can be also significantly affected if creep crack opening exceeds the limit recommended by codes concerning of conventional steel bars. Predicting creep deflection is even more important in the cracked structures exclusively reinforced by fibres. It was shown that the addition of steel fibres to the concrete can limit the long-term crack widening in a cracked section, since fibres restrain the crack growth [5, 6]. However, the crack restraint effectiveness depends on the time evaluation of the sliding process of the fibre pull-out. Under a sustained load, the time-dependent crack widening has been attributed to two main mechanisms: creep behaviour of fibre/matrix interface, and time-dependent fibre creep. In the case of steel fibre composites, the latter contribution can be negligible due to the relatively low shear level induced in the fibre and its high axial stiffness. On the other hand, the long-term crack widening can be ascribed mainly to the long-term fibre/matrix bond mechanisms, which depends on several factors such as: quality of matrix, bond strength, fibre embedment length, fibre geometry, fibre anchorage mechanism, fibre orientation, etc.

Intensive research is currently being undertaken to characterize the serviceability performance of cracked SFRC elements. The durability improvement of the cracked SFRC can be maintained if the crack does not significantly widen under a sustained load. In the literature there are some studies regarding the time-dependent behaviour of FRC, in the cracked state, using either synthetic [7, 8] or steel [9, 10] fibres. It was reported that a lower creep crack opening was observed in concrete reinforced with steel fibres than synthetic fibres. In the case of FRC reinforced with synthetic fibres, for a same pre-cracking and loading level, a relatively large crack widening (i.e. around 0.8 mm) over three

months was reported [11, 12], while in FRC with steel fibres a considerably lower crack opening (i.e. about 0.02 mm) was obtained [5, 6, 9]. To the authors' best knowledge, only a limited number of studies are dedicated to time-dependent fibre pull-out behaviour. In the works of Babafemi *et al.* and Boshoff *et al.* [11, 12], aligned synthetic fibres (i.e. fibres perpendicular to the crack plane) were pulled-out just in a few hours after the loading initiation, even when they were loaded with just 50% of the fibre's bond strength. It is well acknowledged that the orientation of the fibres relative to the crack plane has an important influence on the pull-out behaviour of a single fibre and, consequently, on the FRC tensile behaviour [3, 13]. In fact, understanding the time-dependent modifications at the fibre / matrix interfacial zone of a single fibre (meso-level) can render a better understanding of the creep behaviour of SFRC at the composite level.

In the present work an experimental programme that aims to study the time-dependent pull-out behaviour of a single fibre is presented and discussed. For this purpose, cylindrical concrete specimens containing a single fibre with an embedment length of l_f /4, l_f being the fibre length [14], and distinct inclinations were produced. For each series, the influence of the fibre orientation angle (0, 30 and 60º, see Fig. 1), as well as the pre-imposed fibre slip levels, s_{pr}, 0.3 and 0.5 mm on the pull-out behaviour are appraised. In a first stage, the fibres were subjected to a monotonic pull-out test up to the desired pre-slip level, s_{pr}. Afterwards, the creep pull-out test was carried out under a sustained load until the stabilization of the long-term slip. The specimens used in the pull-out creep tests were then subjected to a quasi instantaneous pull-out test until failure. Finally, a series of quasi instantaneous single fibre pull-out tests were also executed on undamaged specimens (without any pre-slip level), in order to quantify the influence of the long-term slip on the pull-out residual force evolution.

At the composite level, the authors also performed an extensive experimental programme on prismatic specimens extracted from a 1500 × 1500 × 60 mm^3 SFRSCC panel [15]. The specimens were notched in distinct directions towards the expected concrete flow direction, in order to study the influence of fibre distribution and orientation on the composite's long-term behaviour. Therefore, prismatic specimens with different preferential fibre orientations were extracted and subjected to pre-cracking, creep and post-creep tests. The results of the present study in meso-level will be of quit important to cross-link the conclusions obtained at the composite scale. Moreover, the following results will be also used to predict the flexural creep behaviour of panels assuming SFRSCC as a two-phase material comprising one homogeneous phase representative of aggregates and paste, and a second phase that includes all the discrete fibres. It was already observed that with a realistic prediction of the actual fibre distribution/orientation and

having the knowledge of the micro-mechanical behaviour of a single fibre obtained from fibre pull-out test, the mechanical behaviour of the SFRSCC at the composite level can be realistically predicted [16, 17].

2. EXPERIMENTAL PROGRAMME

2.1. Concrete mixture

A self-compacting concrete composition was developed with the constituents included in Table 1. To guarantee the required workability, a third generation Superplasticizer Sika® 3005 (SP) was used. Crushed granite coarse aggregates with a maximum aggregate size of 12 mm were used. The concrete properties in the fresh state were determined by the Abrams cone slump test in the inverted position according to the recommendation of EFNARC [18], having been obtained an average spread of 590 mm. Hooked-end steel fibres with a length, l_f, of 33 mm; diameter, d_f, of 0.55 mm; aspect ratio, l_f/d_f, of 60 and yield stress of 1100 MPa, were used.

The compressive strength of the hardened concrete was assessed by testing six cylinders with a diameter of 150 mm and a height of 300 mm at the age of 28 days according to the ASTM-C39 [19] recommendations. The specimens were cast and stored in a climatic chamber room under 20ºC and 60% relative humidity. Moreover, these specimens were stored in the same climatic conditions in which the creep pull-out tests were performed. The average compressive strength was 72 MPa with a coefficient of variation (CoV) of 8.23 %, while the average Young's modulus was 42.15 GPa with CoV of 0.26 %. The strength class of the SFRSCC was selected in order to achieve a post-cracking flexural performance required for its use on elevated SFRC slabs (supported on columns) in terms of flexural and punching capacity [20-22].

2.2. Specimens

The pull-out tests were undertaken on single sided cylindrical concrete specimens. For this purpose, a special mould was used allowing the production of 81 specimens at the same time with the desired fibre's embedment length and orientation, see Fig. 2a. The bottom surface of the mould consists of ten steel strip shape pieces. Before assembling the mould, fibres were placed with the desired embedment length and inclination in the grooves of the lateral face of

the steel strip pieces, respectively with 0, 30 and 60° (Fig. 2b). Hence, the embedment length of the fibre was located in the bottom zone of the cast panel (Fig. 2a and 2c), without relevant segregation of the concrete constituents due to the relatively small thickness of the panel and proper design mix. Afterwards, the mould was cast as shown in Fig. 2c. The casting procedure was performed carefully, from the centre of panel, in order to prevent any undesired fibre's warping. After curing of concrete, the panel was demoulded, turned over, and cylindrical cores comprising a single fibre were extracted. Fig. 2d depicts the final produced cylindrical specimen, with actual height and diameter of 80 mm.

Prior to testing, two aluminium plates were attached to the extremity of the fibre, in order to avoid undesired fibre rupture at the grip, since the specimens that were used for assessing long-term pull-out behaviour needed to be fasten three times (for pre-slip, creep and post-creep stages). The aluminium plates were glued using epoxy Sikadur®-32N and stored for at least three days until the curing process of epoxy was completed. Additionally, these aluminium plates also guarantee a negligible slip between fibre and grip, since the grip could be tighten firmly [13].

In this study, inclination angles of 0, 30 and 60° were investigated to assess the influence of fibre orientation on the instantaneous pull-out load – slip (F - s) and long-term slip – time (s_{lt} - t) relationships. Cunha *et al.* [23] concluded that the influence of the fibre embedment length is not as significant as the orientation angle. Therefore, considering that the theoretical average value of a fibre's embedded length, l_{fb}, bridging an active crack is l_f / 4 [14], in the present study a l_{fb} = 8.25 mm was selected in the production of all the pull-out specimens. For each orientation angle, six monotonic and six long-term pull-out tests were undertaken (three for each pre-imposed fibre slip level, s_{pr}). For the series with an inclination angle of 0°, additional specimens were also prepared, namely, six specimens (three for each s_{pr}) for executing monotonic tests with one unloading / re-loading cycle (fibres were loaded until the nominal pre-slipping value, s_{pr}. Then, the specimens were unloaded followed by a monotonic loading until the failure of the specimen); and three supplementary specimens with smooth fibres to be tested in monotonic configuration in order to determine the grade of the hooked end mechanical anchorage mobilization. Therefore, a total of forty five specimens were tested.

2.3. Test set-up

2.3.1. Instantaneous fibre pull-out test

2.3.1.1. Monotonic test

The instantaneous fibre pull-out load – slip relationship, F - s, was acquired by using a universal testing rig with a load capacity of 50 kN. Since the peak pull-out loads were relatively low, a load cell with high accuracy was used, namely, a HBM® type S9 load cell with a capacity of 5kN. This load cell was interposed between the servo-actuator and the grip, see Fig. 3a.

The single sided pull-out specimen was accommodated in a steel frame. This frame incorporated one bottom steel plate bolted to the machine testing frame and a steel ring mounted on the upper side of the specimen to fix it. The steel ring was connected to the bottom steel plate using three screws disposed around the specimen forming an angle of 120°. The diameter of both specimen (80 mm) and steel ring hole (60 mm) were designed to prevent the application of confinement to the fibre due to development of compressive stress held in the concrete medium surrounding fibre, which could influence the pull-out response.

For measuring the fibre's slip during the pull-out procedure, three Linear Variable Differential Transformers (LVDTs) with linear stroke +/- 5 mm were installed on the back side of grip using aluminium cubic supports to exclude measuring deformation of the test rig, Fig. 3b. Moreover, to assess the fibre slip at the grip, a VMS-004D-400x USB Microscope camera with a 2 Mega Pixels resolution was also used. For the adopted test set-up the fibre slippage at the grip was negligible, lower than 4 μm. The test was controlled by an LVDT installed on the actuator, and adopting a displacement rate of 1 μm/s up to the slip of 2 mm, and 4 μm/s until the end of the test. This test control procedure guaranteed a stable response during the test, especially during the debonding process of the fibre.

2.3.1.2. Tests with one unloading / re-loading cycle

To evaluate if an unloading (in pre-slipping test) / re-loading (in post-creep test) cycle will affect the peak load or influence of the long-term slip on the secondary stiffness, a series of tests with one unloading / re-loading cycle was also conducted. In this test, fibres were loaded until the nominal pre-slipping value, s_{pr}, i.e. 0.3 or 0.5 mm. Then, the specimens were unloaded followed by a monotonic loading until the failure of the specimen, see Fig. 4. In this figure,

hereinafter, s_{pr}^{res} denotes as the residual slip after unloading of the specimen, $K_{sec,inst}$ is the instantaneous secondary stiffness at re-loading process, F_p^{max} and s_p^{max} are the maximum load recorded during the test and its correspondent slip, respectively.

2.3.2. Long-term fibre pull-out test

To obtain the long-term *F* - *s* relationship, experimental tests were carried out in three stages: firstly, the fibres were exposed to a pre-slip level of either 0.3 or 0.5 mm; secondly, the creep tests were carried out for the pre-imposed fibre slip specimens until the stabilization of the long-term slip; finally, pull-out tests were performed until the fibre was fully pulled-out.

2.3.2.1. Pre-slipping of the fibre

Prior to the execution of the long-term pull-out tests, each specimen's fibre was subjected to a certain pre-slip level, s_{pr}. The monotonic pull-out test set-up was adopted for pursuing this objective and the fibre was loaded until the average slip in the LVDTs reached the target s_{pr}, and then the specimen was unloaded. Note that the latter slip also comprises a component related to the fibre elongation. In this study, two nominal slip levels were investigated: 0.3 mm that can be correlated to the crack opening width in serviceability limit states [24], and 0.5 mm that was close to the peak pull-out load. After imposing the pre-slip, the specimen was unloaded. Finally, the specimen was carefully removed, in order to avoid any introduction of bending or torsion when unfastening the fibre from the grip.

2.3.2.2 Pull-out creep test

The fibre pull-out creep tests were performed in a climatic chamber room with a fixed temperature of 20°C $\pm$ 0.5 and 60% relative humidity $\pm$ 5% as recommended by ASTM-C512 [25] for the assessment of creep under compression. Before positioning the specimens on the creep table, they were kept in the chamber room for around five hours. For evaluating the long-term performance of the fibre / matrix interface, an innovative test set-up was designed allowing five specimens to be tested simultaneously (Fig. 5a). The test set-up was composed of a creep table, five LVDTs, a

data acquisition system and a computer. In the creep table, a grip, a steel arm that was withheld by a support at a quarter of its length, and a steel bar for supporting the applied weight loads exist for each specimen (Figs. 5b and 5c). The same steel rings used in the monotonic tests were accommodated on the top of the specimen, connected to the table by three bolts. Furthermore, a hinge was used to connect the grip to the steel arm in order to prevent the introduction of bending moment at the fibre, and also to assure that the specimen was loaded in the fibre's axis, see Fig. 5c.

During the creep test, the fibre slip was acquired with an LVDT installed on each grip. The same connection details of the monotonic test set-up were adopted. To evaluate the level of fibre slippage in the grip, a USB Microscope was also used, see Fig. 5c. The fibre slippage at grip was also negligible similar to the monotonic tests. In this test at the time of loading and unloading procedures, the slip was measured within a relatively short time period (one reading per 2 sec) since the slip variation was significant at this stage. To reduce the amount of the recorded data, the intervals between readings was increased, one read-out per 500 and 1000 seconds for the first month and until the completion of the test, respectively.

After the initiation of the creep test, the value of the applied load, F_a, see Fig. 6b, was maintained constant until the long-term slip was stabilized. When the variation of the long-term slip was smaller than one micrometer for three consecutive days, it was assumed that the slip was stabilized, and the test was finalized. In the present research, the load level (F_a / F_{pr}) selected was equal to 100 or 80% of that observed at s_{pr}=0.3 or 0.5 mm in the pre-slip tests, respectively. It should be mentioned that for the specimens with 0° fibre inclination angle, the pre-slip level 0.5 mm was very close to the slip at the peak load. Therefore, in the s_{pr}= 0.5 mm series, to prevent the premature fibre's rupturing or pulling-out at initial stage of creep test, the specimens were subjected to a lower loading level.

After the creep tests were completed, the specimens were unloaded, but the data acquisition system was kept active for at least a period of one week, to also record the recoverable slip component due to the creep recovery process. Figs. 6a and 6b include a schematic representation of slip versus time and force – slip relationship. In these figures, s_{inst} is the instantaneous slip, s_{lt} represents the long-term slip, s_{inst}^{rec} states the instantaneous slip recovery at the beginning of the unloading process, s_{lt}^{rec} represents long-term slip recovery, s_{total}^{rec} is the total slip recovery, s_{lt}^{res} is the residual slip after complete unloading stage, and F_a is the applied load level in creep test.

2.3.2.3 Post-creep test

One week after the creep tests had ended (a waiting period for creep deformation recovery), the specimens were then subjected to a monotonic fibre pull-out test. The monotonic test set-up was similar to the one used for pre-slipping the fibres, which was previously detailed.

2.3.2.4 Assembled long-term force-slip curve

Finally, the complete F - s curves were assembled with the individual F - s curves from the pre-slipping, creep and post-creep responses, as schematically presented in Fig. 7. Then the assembled response was compared with the corresponding curve from the instantaneous monotonic pull-out tests. In Fig. 7, F_{pr} and s_{pr} are the pre-slipping load and corresponding slip value, respectively, s_{pr}^{res} is the residual slip after unloading of the specimen, $K_{sec,lt}$ is the long-term secondary stiffness at re-loading process of post-creep test, $F_p^{\max}$ and $s_p^{\max}$ are the maximum load recorded during the test and its corresponding slip, respectively.

3. RESULTS AND DISCUSSION

3.1. Monotonic fibre pull-out tests

3.1.1. Pull-out load – slip curves

Fig. 8 indicates the average pull-out load versus slip curves and corresponding envelope for the adopted fibre inclinations. The slip was determined by averaging the readouts recorded in the three LVDTs installed on the grip. In all curves, the pre-peak branch was composed of a linear and nonlinear part. The first part is associated to the elastic behaviour of the bond. For the fibres with an inclination angle of 0°, the nonlinear part in the pre-peak branch can be associated to a non-recoverable degradation of the adhesion between the fibre and surrounding matrix, as well as the beginning of the plastic deformation of the hook, Fig. 8a. When the peak load was attained, a relatively smooth load decay was observed. During this softening stage, the fibre mechanical anchorage is progressively mobilized. After a

slip of about 3.5 mm when the hook was completely straightened, the fibre pull-out force is mainly governed by fibre / matrix friction. Due to the reduction of the fibre's embedment length, this stage is characterised by a small decrease of the pull-out force during the imposed slip process.

Fig. 8b shows the load – slip curve for fibres with an inclination angle of 30°. The average curve was depicted up to the slip where the fibre rupture has occurred. The pre-peak branch is similar to the fibres with 0° angle, but a slightly lower value of peak load was attained. The nonlinear part was slightly less stiff due to the cracking and spalling of the matrix occurred at this fibre exit point due to the deviational force component that fibre applies to this medium [26].

Fig. 8c indicates the pull-out load – slip response for the 60° series. In similarity to the 30º series, the specimens failed by fibre rupture. When the fibre inclination angle increases, the matrix at the fibre exit point is more prone to cracking and spalling due to the higher deviational force component applied by the fibre. The nonlinear component of the first branch is of small significance until the first evidence of matrix spalling. Afterwards, a matrix wedge was formed and gradually detached. The fibre segment embedded under this concrete portion was straightened, which corresponds to the plateau in the pull-out load – slip relationship where the slip increases under an approximately constant load. However, in some specimens a sudden reduction in the load was also recorded once the matrix has spall. After the wedge had fully detached, a new equilibrium was attained and the pull-out fibre process continued with a smaller stiffness until the fibre rupture, which occurred at a load level lower than in the two previous series.

The maximum monotonic pull-out load decreased with the increase of the inclination angle as already observed in other experimental programs. The tensile stress of fibre rupture (computed as the ratio between load and the fibre net cross sectional area), for 30 and 60° inclination angles were 993 and 840 MPa, respectively. This is justified by the fact that the fibre is subjected to a mixed tensile-bending mode as well as to shear stresses due to the deviational force component. Regarding the slip at peak load, it was observed that $s_p^{\max}$ has decreased slightly for an inclination angle of 30°, and then has increased significantly for 60° specimens. This significant increase of $s_p^{\max}$ is caused by spalling of the matrix at the fibre exit point [27]. On the other hand, when the orientation angle increases, a bigger portion of concrete is pushed off at the fibre's exit point, hence a larger fibre's protruding length is straighten, leads to an additional slip component. Consequently, in the case of large inclination angles, similar to 60°, the slip included an important increment due to the fibre deformation.

3.1.2. Mechanical contribution of the hooked end

In general, for the hooked end fibres, fibre/matrix bond consists of three components: the first one is related to the adherence between paste and fibre (hereinafter known as chemical bond), the other is concerned with the mechanical component due to the yield of the hook during slipping throughout the concrete channel, and the last one is fibre/matrix friction. Fig. 9 includes the average load – slip relationships of the hooked end and smooth fibres for the 0º series. Moreover, the estimated contribution of the end hook to the overall pull-out behaviour is also depicted, which was determined by subtracting the smooth fibre average curve from the hooked fibre average curve. This assessment was performed exclusively for the 0° series, since for inclined fibres other factors are involved such as a supplementary frictional resistance due to the force component normal to the fibre axis, bending and plastification on the exiting point of the fibre; spalling of the concrete near to the fibre bending point [23]. The component correspondent to the chemical adherence between paste and fibre played a small role in the overall pull-out response, which was principally governed by the mechanical bond. Considering the maximum pull-out load, the contribution of the chemical and mechanical bonds were, respectively, 16% and 84%. Furthermore, by considering the response of smooth fibres, it was also observed that the chemical bond was exhausted at a slip of 0.06 mm. Thus, for the investigated pre-slip levels, s_{pr}=0.3 and 0.5 mm, the chemical bond was already fully exhausted, and fibre pull-out mechanism is governed by mechanical bond provided by the hook anchorage mechanism.

3.1.3. Instantaneous test with one unloading / re-loading cycle

Fig. 10 shows the average cyclic pull-out load – slip relationships for fibres with inclination angle of 0°. A peak pull-out load of 251 and 257 N for pre-slip levels of 0.3 and 0.5 mm, respectively, was observed. Comparing these values with the average values obtained from the monotonic tests (254 N), see Fig. 8a, it can be concluded that the maximum pull-out load of fibre is not influenced by the application of an unloading and re-loading cycle. The average instantaneous secondary stiffness, $K_{sec,inst}$, was also determined according to the schematic representation in Fig. 4. Values of 1.70 and 1.61 kN/mm for pre-slip levels of 0.3 and 0.5 mm, respectively, were determined. As it was expected, $K_{sec,inst}$ has decreased with the increase of the pre-slip level but quite moderately.

3.2. Long-term fibre pull-out tests

3.2.1. Creep parameters

Tables 2 and 3 show the average slip rate, *SR*, and average creep coefficient, ϕ^C , respectively, for each s_{pr} at 7, 15, 30 and 60 days from starting time of the creep test. The slip rate and creep coefficient were calculated from the following equations:

$$SR_{t_2-t_1} = \frac{s_{lt}^{t2} - s_{lt}^{t1}}{t_2 - t_1} \tag{1}$$

$$\phi_{ti}^{C} = \frac{s_{lt}^{ti}}{s_{inst}} \tag{2}$$

where, $SR_{t_2-t_1}$ is the slip rate between time t_2 and t_1, s_{lt}^{ti} represents the long-term slip at time t_i, ϕ_{ti}^{C} is creep coefficient at time t_i and s_{inst} is the instantaneous slip at loading application (Fig. 6). For instance, the slip rate between 15 to 7 days (SR_{15-7}) is determined as $\left(s_{lt}^{15} - s_{lt}^{7}\right)/(15-7)$, whereas the creep coefficient at 15 days (ϕ_{15}^{C}) is calculated as s_{lt}^{15}/s_{inst} . For s_{pr} = 0.5 mm series, the creep test could not be performed on the specimens with a fibre inclination angle of 30°, because the fibres had ruptured during the execution of the instantaneous pull-out tests at an average slip of 0.47 mm. For all specimens, it was observed that the highest slip rate occurred during the first week, and continuously decreased over time. At 60 days of testing, the slip rate became smaller than the test stopping criteria, which means that the long-term slip stabilized after a period of two months. Similar findings were also observed for the creep coefficients.

Fig. 11 includes the average and envelope of the long-term slip, s_{lt}, versus time values for each fibre orientation angle and pre-slip level, up to a period of two months. Similar to what was observed in composite level [15], all series have shown a two-stage creep response, namely, primary and secondary stages, in which the long-term slip was increased importantly with time and then followed by a steady state part where the increment in slip was not so predominant. However, in s_{pr} = 0.5 mm series, the slip was stabilized in a higher time period. It should be worth noted that the former specimens subjected to a higher level of damage in the bond between fibre/matrix, therefore slip was stabilized

in a higher time period. Under the sustained load, none of the specimens reached the tertiary creep stage, i.e. unstable creep response, where long-term slip increases in time sharply until fully extraction of the fibre.

3.2.2. Influence of the fibre orientation on the creep parameter

Fig. 12 shows the long-term slip versus time relationship for distinct fibre orientation angles. Fibre orientation has an important effect on the long-term slip, since a clear increase of s_{lt} with the decrease of fibre inclination was obtained. This tendency seems to increase with the s_{pr} applied. This can be clearly concluded from the results showed in Fig. 13. In the series of s_{pr} = 0.3 mm and fibre inclination angle of 0° at 60 days time lapse, the long-term slip was 19% and 69% higher than in the case of fibre orientation angles of 30 and 60°, respectively. Regarding the series s_{pr} = 0.5 mm, the fibre orientation effect is even more pronounced (Fig. 13b) since at 60 days time lapse, the long-term slip of fibre at 0° was 135% larger than at 60°. The different failure modes observed in the specimens with fibres differently oriented can contribute for this behaviour. As was explained earlier, in section 3.1, for specimens with inclination angle of 0°, the fibre was fully pulled-out whereas for 60° orientation angle, the pull-out response was mainly governed by matrix spalling and finally fibre rupturing. In the case of inclined fibres (30 and 60°), a compressive stress field exists at the fibre bending point, which applied by the deviational force component of the fibre. Considering the Mohr-Coulomb effects, the fibre slippage is also resisted by the shear friction that increases with a normal stress field installed in the fibre exit point. However, for a fibre with 0° inclination angle since it is subjected to only direct tensile loading (without any deviational force component), therefore it is more susceptible to be pulled-out under a sustained load than other series. From another point of view, for the 0° series, s_{pr} = 0.5 mm was very close to the slip correspondent to the peak load, $s_p^{\max}$. On the other hand, by comparing the ratio of the applied load in creep test to the maximum load recorded during pull-out test, $F_a / F_p^{\max}$, see Table 4, in average terms, this coefficient was 81% and 39% for 0° and 60° orientation angles, respectively. Therefore, loading specimens to a level close to the maximum load carrying capacity of the specimen provides the development of higher long-term slip under a sustained load, confirming the results already obtained in this respect in macro-level [15].

3.2.3. Influence of pre-slip level on the creep parameter

Fig. 14 shows the influence of the pre-slip level on the long-term slip – time responses. Considering specimens with 0° fibre orientation angle, the long-term slip increased significantly with s_{pr}. From Fig. 9, it was observed that for the both studied pre-slip values, the chemical bond was completely exhausted and the debonding of the hooked end has already started. Moreover, it is also observed that for a slip of 0.3 mm the fibre's hook was partially debonded, whereas for s_{pr}=0.5 mm a higher debonding force is expected at the fibre's hook. Therefore, in s_{pr} = 0.5 mm specimens, the bond between the fibre/matrix had already a higher level of damage, consequently a higher long-term slip due to the creep behaviour was observed. An increase of 50% on the long-term slip was observed for the fibres pre-slipped up to 0.5 mm when compared to the s_{pr} = 0.3 mm series. On the other hand, the series with a 60° angle have shown a distinct behaviour. By increasing the pre-slip from 0.3 mm to 0.5 mm, the long-term slip had a slight increase. From Fig. 8c it is observed that both studied pre-slip levels were positioned in the plateau part of the monotonic pull-out response of the 60º series, in which the slip increased at an almost constant load. Therefore, the achieved pre-slipping load, F_{pr}, for both investigated pre-slip levels was relatively similar. In the long-term pull-out tests, considering the selected loading levels for each series, the specimens of the 0.5 mm series were subjected to a lower load, F_a, see Table 4. Hence, it is rational to expect that the creep response for this series exhibited a response similar to that of the 0.3 mm series, even though s_{pr} =0.5 mm series endured a higher level of damage at the fibre/matrix interface. From another point of view, when having in mind the maximum monotonic pull-out load, the s_{pr} = 0.3 mm series were subjected to a loading level of $F_a / F_p^{\max} = 54\%$, whereas the s_{pr} = 0.5 mm series the loading level was just 39%.

3.4 Comparison between monotonic, cyclic and long-term results

Considering fibres with a 0° degree inclination, a small reduction on the instantaneous secondary stiffness, $K_{sec,inst}$, obtained from cyclic test (Fig. 4) can be observed when compared to the long-term secondary stiffness, $K_{sec,lt}$ (Fig. 7), determined from the post-creep test. The average $K_{sec,lt}$ was 1.51 and 1.41 kN/mm for the series with pre-slip levels of 0.3 and 0.5 mm, respectively. When comparing to the $K_{sec,inst}$ a 12.6% and 14.2% reduction was observed for the 0.3 and 0.5 mm series, respectively. This could provide corroborating evidence that the creep phenomenon had a minor detrimental influence on the interfacial bond between fibre and matrix [15].

Fig. 15 includes both the monotonic and long-term pull-out assembled curves for each fibre orientation category and s_{pr}. These responses were obtained by averaging all the corresponding curves. The full response relationship is obtained by overlaying the force – slip curves from the tests corresponding to: the specimen's pre-slipping, creep, and post-creep tests, as schematically represented in Fig. 7. The development of the long-term slip has a minor influence on the post-creep residual forces. It is evident that the assembled curves resemble quite well the average responses of the monotonic tests. Nevertheless, in some cases, due to the scatter of the test results, the assembled responses did not follow so closely the average monotonic curves, nonetheless, they are yet comprised within the experimental envelope of the monotonic pull-out tests.

4. EMPIRICAL APPROACH TO PREDICT TIME – DEPENDENT FIBRE PULL-OUT BEHAVIOUR

In this section, the experimental results presented in section 3.2 were used to calibrate empirical equations to predict the long-term response of the pre-slipped fibre pull-out specimens. For each fibre inclination angle series, the influence of s_{pr} and F_a / F_{pr} parameters were taken into account in the present approach. A combined power and hyperbolic equation was used, since similar equations were already proposed by ACI 209-92 [28] and CEB [29] to predict creep behaviour of plain concrete under compression behaviour. The following equation is proposed for predicting the time-dependent fibre pull-out behaviour:

$$s_{lt} = \frac{t^A}{B + t^A} \times c \tag{3}$$

where s_{lt} is long-term slip (in mm), and t presents the time duration of loading (in hours). According to the experimental data, parameters A and B are determined by:

$$A = s_{pr}\left(1.5 - 1/F\right) + d \tag{4}$$

$$B = 1 \Big/ \left(0.047 s_{pr}\right) \tag{5}$$

where s_{pr} is the pre-slip value (in mm) and F represents the normalized level of loading (F_a / F_{pr}). In Eqs. (3) and (4) constants c and d were determined by nonlinear curve fitting analysis procedures. The coefficient c depends on the

fibre orientation angle and the following values were proposed: 1, 0.72 and 0.45 (R-square values: 0.96, 0.95 and 0.97) for fibre orientation angles 0°, 30° and 60°, respectively. Furthermore, coefficient *d* was also determined as 0.11 (R-square value of 0.96) for all series. It should be mentioned that Eq. (3) is only valid for $0.6 \leq F_a / F_{pr} \leq 1.0$. Fig. 16 compares the long-term slip versus time obtained from the empirical expressions and the corresponding experimental ones. Since the equations where calibrated by assigning the obtained experimental data and considering that relatively high R-square values where achieved, it is natural that high predictive performance is obtained when compared the experimental and empirical results. However, to properly validate the proposed equations more experimental data is required, with of the pre-slip values, load levels, and higher time periods.

Figs. 17a to 17e depict the results of a parametric study to investigate the influence of pre-slip value (s_{pr}=0.3 and 0.5 mm) and also the load level (F_a / F_{pr} = 0.6, 0.7, 0.8, 0.9 and 1.0) on the long-term slip, s_{lt}, versus time response up to a period of one year. In general, the long-term slip increased with the increase of the F_a / F_{pr} ratio, and this increase was more significant for higher values of s_{pr}. Considering now the influence of s_{pr} on the long-term slip, for the same fibre inclination angle and F_a / F_{pr} it was observed that the increase of s_{pr} led to an increase of the long-term slip, mainly for the higher load levels.

5. CONCLUSIONS

In the present research, the effectiveness of a fibre as an element for transferring stresses under a sustained load across a crack was assessed by performing single fibre pull-out creep tests, in which the fibre slip was monitored as a function of time and pull-out load. For this purpose, cylindrical specimens with a single fibre located in the centre were cast with distinct fibre inclination angle, and monotonic and long-term pull-out tests were carried out. The influence of the fibre inclination angle and the pre-imposed fibre slip levels on the long-term pull-out behaviour was studied. Finally, the assembled long-term curves comprising the pre-slipping, creep and post-creep responses were compared to the correspondent monotonic ones.

In general, two fibre failure modes were observed during monotonic pull-out tests. In the case of the fibres with inclination angle of 0°, the complete fibre pull-out was observed, whereas for the inclined fibres, fibre rupture was the predominant failure mode. The maximum monotonic pull-out load decreased with the increase of the inclination angle,

while the slip at peak load, in general, increased with the angle. This increase of slip at peak load could be ascribed to other additional mechanisms in the pull-out process, which include the matrix spalling and fibre deformation.

Considering the long-term pull-out tests for both investigated pre-slip levels, i.e. 0.3 and 0.5 mm, stable responses were obtained for all series. Regarding the influence of the pre-slip levels, the s_{pr}= 0.5 mm series showed a higher long-term slip comparing to the s_{pr}= 0.3 mm series. Since in the applied pre-slip of 0.5 mm, the interface bond between fibre and matrix was more deteriorated, therefore the long-term slip has increased in a higher rate.

The creep behaviour of the specimens was influenced by the fibre orientation angle. For the time period considered (60 days), fibres with 0° orientation angle showed the highest long-term slip, whereas the lowest long-term slip was observed for the 60° specimens. This was due to the different failure modes of these specimens. In the case of inclined fibres, the fibre slippage is also resisted by the shear friction that increases with a normal stress field installed in the fibre exit point. However, for a fibre with 0° inclination angle since it is subjected to only direct tensile loading (without any deviational force component), therefore it is more susceptible to be pulled-out under a sustained load than other series. From another point of view, by comparing the ratio of the applied load in creep test to the maximum load recorded during the test, F_a / $F_p^{\max}$, 0° specimens were subjected to a higher loading level.

In general, the fibre pull-out behaviour registered after the specimens have been subjected to long-term pull-out tests was not significantly affected, when the behaviour obtained from instantaneous monotonic tests is taken for comparison purposes, even when the specimens were pre-slipped nearby the slip corresponding to the maximum pull-out load.

Based on the results obtained from the creep tests, an empirical equation was proposed to predict the evolution of the long-term slip with time. The proposed equation is able to estimate the experimental results with high accuracy, and seems capable of estimating the $s_{lt} - t$ for hooked end steel fibres up to 0.5 mm and loaded within the interval $0.6 \leq F_a / F_{pr} \leq 1.0$. However, further research is required to appraise its capability to predict the behaviour of other steel fibres, pre-slip levels, F_a / F_{pr} values, fibre orientations and embedded lengths as well as concrete strength classes.

ACKNOWLEDGEMENTS

This work is supported by the FEDER funds through the Operational Program for Competitiveness Factors - COMPETE and National Funds through FCT - Portuguese Foundation for Science and Technology under the project

SlabSys-HFRC-PTDC/ECM/120394/2010. The authors would like to acknowledge the materials supplied by Radmix and Maccaferri (fibres), SECIL (cement), SIKA and BASF (superplasticizers), Omya Comital (limestone filler), and Pegop (Fly ash).

REFERENCES

[1] Barnett SJ, Lataste JF, Parry T, Millard SG, Soutsos MN. Assessment of fibre orientation in ultra-high performance fibre reinforced concrete and its effect on flexural strength. Mater Struct 2010;43:1009-1023.

[2] Kang ST, Kim JK. The relation between fibre orientation and tensile behavior in an ultra high performance fiber reinforced cementitious composite (UHPFRCC). Cem Concr Res 2011;41:1001-1014.

[3] Abrishambaf A, Barros JAO, Cunha VMCF. Relation between fibre distribution and post-cracking behaviour in steel fibre reinforced self-compacting concrete panels. Cem Concr Res 2013;51:57-66.

[4] Abrishambaf A, Barros JAO, Cunha VMCF. Tensile stress-crack width law for steel fibre reinforced self-compacting concrete obtained from indirect (splitting) tensile tests. Cem Concr Compos 2015;57:153-165.

[5] Tan KH, Paramasivan P, Tan KC. Creep and shrinkage deflections of RC beams with steel fibres. ASCE J Mater Civ Eng 1994;6:474-494.

[6] Tan KH, Saha MK. Ten year study on steel fibre-reinforced concrete beams under sustained loads. ACI Struct J 2005;3:472-480.

[7] Al-Khaja WA. Mechanical properties and time-dependent deformation of polypropylene fibre reinforced concrete. J King Saud Univ Eng Sci 1995;7:67-76.

[8] Kurt S, Balaguru P. Post crack creep of polymeric fibre-reinforced concrete in flexure. Cem Concr Res 2000;30: 183-190.

[9] Mouton CJ, Boshoff WP. Initial study on the tensile creep of cracked steel fibre reinforced concrete. 8th RILEM Internatinal Symposium on Fibre Reinforced Concrete: Challenges and Opportunities. Guimarães, Portugal, 2012.

[10] Zhao G, Prisco MD, Vandewalle L. Experimental research on uni-axial tensile creep behaviour of pre-cracked steel fibre reinforced concrete. 8th RILEM Internatinal Symposium on Fibre Reinforced Concrete: Challenges and Opportunities, Guimaraes, Portugal, 2012.

[11] Babafemi AJ, Boshoff WP. Tensile creep of macro-synthetic fibre reinforced concrete (MSFRC) under uni-axial tensile loading. Cem Concr Compos 2014;55:62-69.

[12] Boshoff WP, Mechtcherine V, Zijil GPAG. Characterising the time-dependent behaviour on the single fibre level of SHCC: Part 1: Mechanism of fibre pull-out creep. Cem Concr Res 2009;39:779-786.

[13] Cunha VMCF, Barros JAO, Sena-Cruz JM. Pullout behaviour of steel fibres in self-compacting concrete. Mater Civ Eng 2010;22:1-9.

[14] Stroeven P, Hu J. Effectivness near boundaries of fibre reinforcement in concrete. Mater Struct 2006;39:1001-1013.

[15] Abrishambaf A, Barros JAO, Cunha VMCF. Time-dependent flexural behaviour of cracked steel fibre reinforced self-compacting concrete panels. Cem Concr Res 2015;72:21-36.

[16] Abrishambaf A, Cunha VMCF, Barros JAO. A two phase material approach to model steel fibre reinforced self-compacting concrete in panels. Eng Fract Mech 2016;162:1-20.

[17] Cunha VMCF, Barros JAO, Sena-Cruz JM. A finite element model with discrete embedded elements for fibre reinforced composites. Comput & Struct 2012;94:22-33.

[18] EFNARC. The European guidelines for self-compacting concrete, 2005.

[19] ASTM-C39. Standard test method for compressive strength of cylindrical concrete specimens, Annual Book of ASTM Standards. American Society of Testing Materials, 2014.

[20] Salehian H. Evaluation of the performance of steel fibre reinforced self-compacting concrete in elevated stab systems: from the material to the structure. Civil Engineering Department, University of Minho, Portugal, 2015.

[21] Soltanzadeh F, Barros JAO, Santos RFC. High performance fiber reinforced concrete for the shear reinforcement: experimental and numerical research. Constr Build Mater 2015;77:94-109.

[22] Barros JAO, Moraes-Neto BN, Melo GSSA, Frazão CMV. Assessment of the effectiveness of steel fibre reinforcement for the punching resistance of flat slabs by experimental research and design approach. Compos Part B 2015;78:8-25.

[23] Cunha VMCF. Steel fibre reinforced self-compacting concrete: from micromechanics to composite behaviour. Civil Engineering Department, University of Minho, Portugal, 2010.

[24] EN 1992-1-1. Eurocode 2: Design of Concrete Structures. European Committee of Standardization, Brussels, 2004.

[25] ASTM-C512. Standard Test Method for Creep of Concrete in Compression. American Society of Testing Materials, 2004.

[26] Laranjeira F. Design-oriented constitutive model for steel fiber reinforced concrete. Universitat Politècnica de Catalunya, Spain, 2010.

[27] Soetens T, Van Gysel A, Matthys S, Taerwe L. A semi-analytical model to predict the pull-out behaviour of inclined hooked-end fibres. Constr Build Mater 2013;43:253-265.

[28] ACI-Committee-209. Prediction of creep, shrinkage and temperature effects in concrete structures. ACI Manual of Concrete Practice, Part 1, 1997.

[29] CEB-FIP. Model code for concrete structures: Evaluation of the time dependent behaviour of concrete. Comite European du Beton/Federation Internationale de la Precontrainte, Lausanne Bulletin d'Information No. 199, 1999.

FIGURES AND TABLES

List of Figures:

Fig.1: Definition of the studied fibre orientation angles.

Fig. 2: Production of the specimens for fibre pull-out test program: (a) casting device, (b) fibres installation in mould, (c) cast panel and (d) extracted pull-out specimen.

Fig. 3: Configuration of single fibre pull-out test: (a) details of the test, (b) connection details of the LVDTs.

Fig. 4: Schematic response obtained from the instantaneous pull-out test with one unloading / re-loading cycle.

Fig. 5: Fibre pull-out creep test: (a) general view, (b) loading details, and (c) specimen installation details.

Fig. 6: Definition of the slip parameters in pull-out creep response: (a) slip – time relationship, s - t, (b) force – slip, F - s.

Fig. 7: Schematic representation of the assembled long-term force – slip curve.

Fig. 8: Average monotonic pull-out load versus slip relationships for fibre inclination angles of: (a) 0°, (b) 30°and (c) 60°.

Fig. 9: Contribution of the end hook to the overall pull-out behaviour in fibres with inclination angle of 0°.

Fig. 10: The average cyclic pull-out load – slip relationships for fibres with inclination angle of 0° and s_{pr} equals to: (a) 0.3 mm, and (b) 0.5 mm.

Fig. 11: Long-term slip versus time during fibre pull-out creep test: (a) and (b) 0 degree, (c) 30 degree, (d) and (e) 60 degree; (a), (c), (d) s_{pr} = 0.3 mm and (b), (e) s_{pr} = 0.5 mm.

Fig. 12: Long-term slip versus time for different fibre orientations and s_{pr} equal to: (a) 0.3 mm, and (b) 0.5 mm.

Fig. 13: Influence of fibre orientation angle on the long-term slip for s_{pr} equal to: (a) 0.3 mm, and (b) 0.5 mm.

Fig. 14: Influence of pre-slip level on the development of long-term slip along time.

Fig. 15: Comparison of monotonic and long-term assembled curves: (a) and (b) 0 degree, (c) 30 degree, (d) and (e) 60 degree; (a), (c), (d)s_{pr} = 0.3 mm and (b), (e) s_{pr} = 0.5 mm.

Fig. 16: Comparison between experimental and analytical long-term slip vs. time relationship for series with fibre inclination angle: (a) 0°, (b) 30° and (c) 60°.

Fig. 17: Influence of F_a / F_{pr} on the long-term slip vs. time response for s_{pr} equal to: (a), (c), (d) 0.3 mm and (b), (e) 0.5 mm; fibre inclination angle of: (a), (b) 0° and (c) 30° and (d), (e) 60°.

List of Tables:

Table 1: Mix constituents of self-compacting concrete per m^3.

Table 2: Average slip rate for each pre-slip level (numbers in parenthesis represent CoV in %).

Table 3: Average creep coefficient at creep stage for each pre-slip level (numbers in parenthesis represent CoV in %).

Table 4: The average applied load in creep test (F_a) and the maximum load recorded during the pull-out test (F_{max}) for each series of specimens.

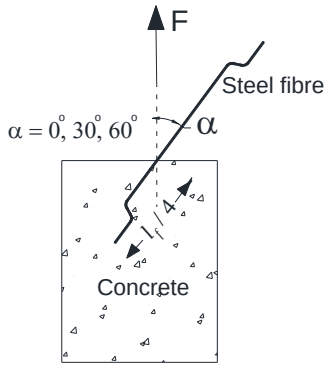

Fig.1: Definition of the studied fibre orientation angles.

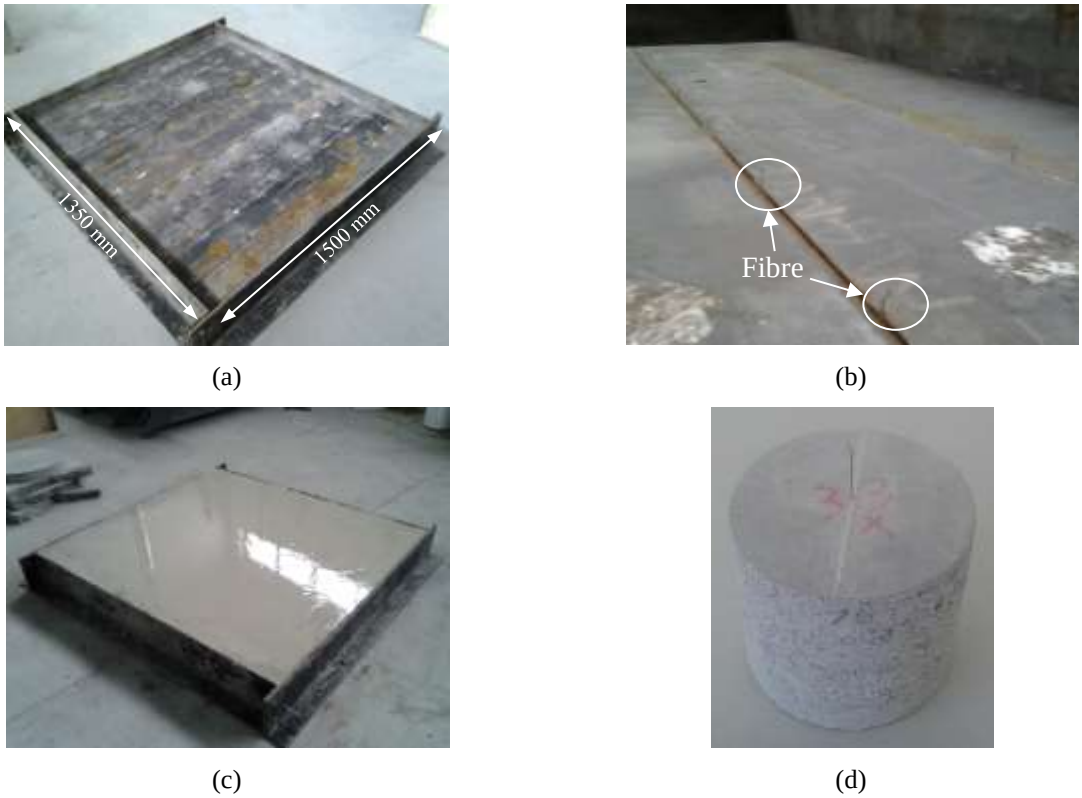

Fig. 2: Production of the specimens for fibre pull-out test program: (a) casting device, (b) fibres installation in mould, (c) cast panel and (d) extracted pull-out specimen.

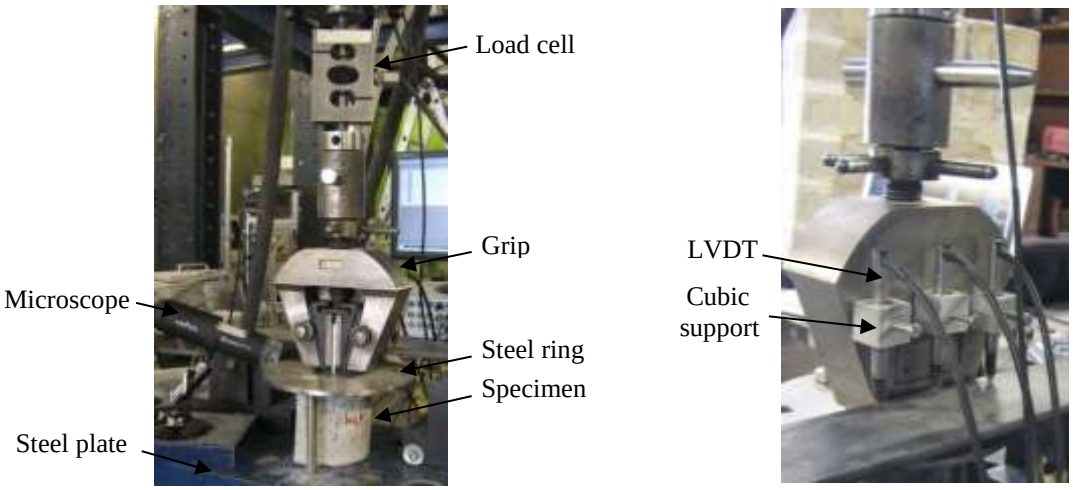

Fig. 3: Configuration of single fibre pull-out test: (a) details of the test, (b) connection details of the LVDTs.

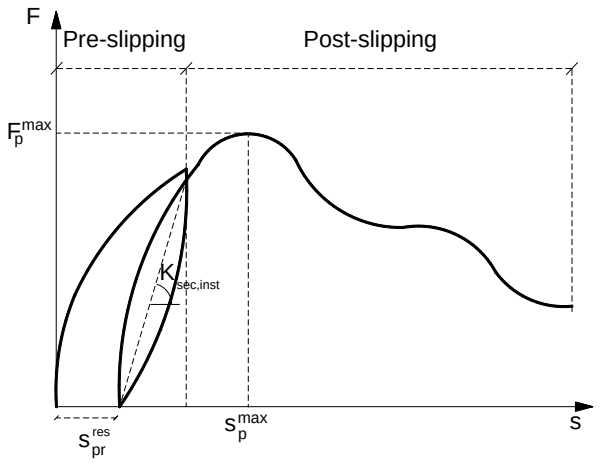

Fig. 4: Schematic response obtained from the instantaneous pull-out test with one unloading / re-loading cycle.

(a)

(b)

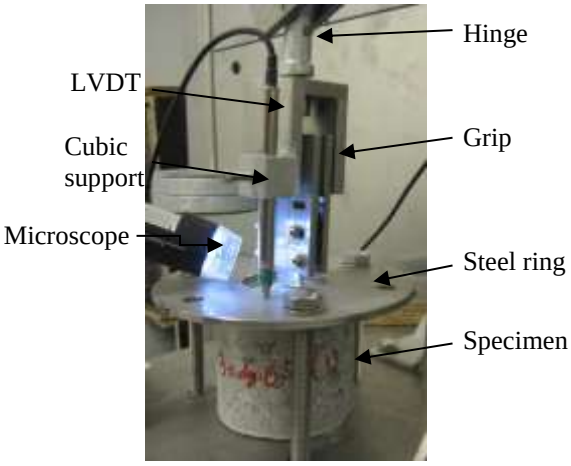

(c)

Fig. 5: Fibre pull-out creep test: (a) general view, (b) loading details, and (c) specimen installation details.

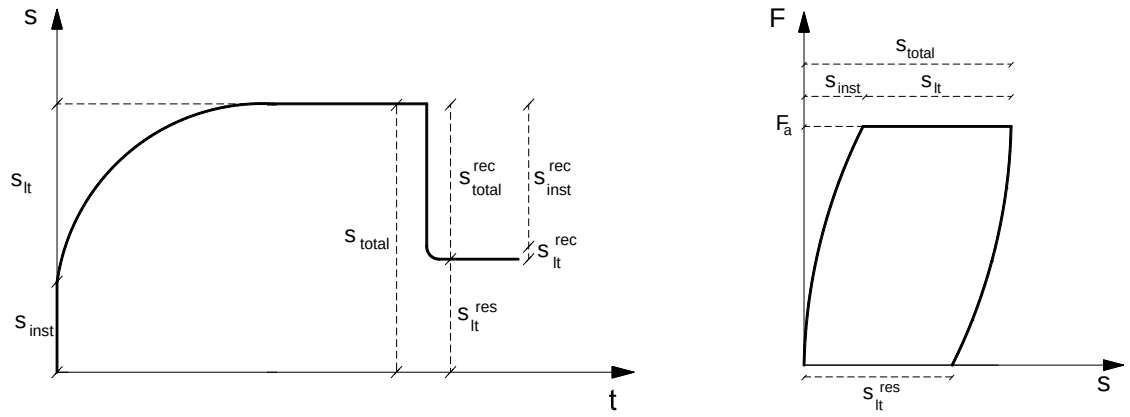

(a) (b)

Fig. 6: Definition of the slip parameters in pull-out creep response: (a) slip – time relationship, *s* - *t*, (b) force – slip, *F* - *s*.

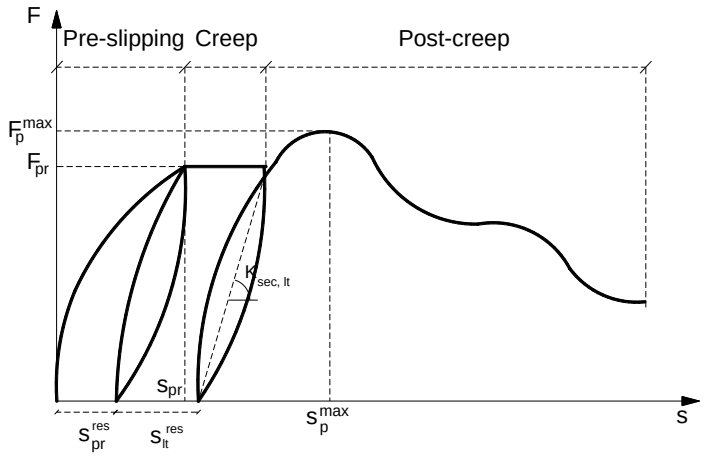

Fig. 7: Schematic representation of the assembled long-term force – slip curve.

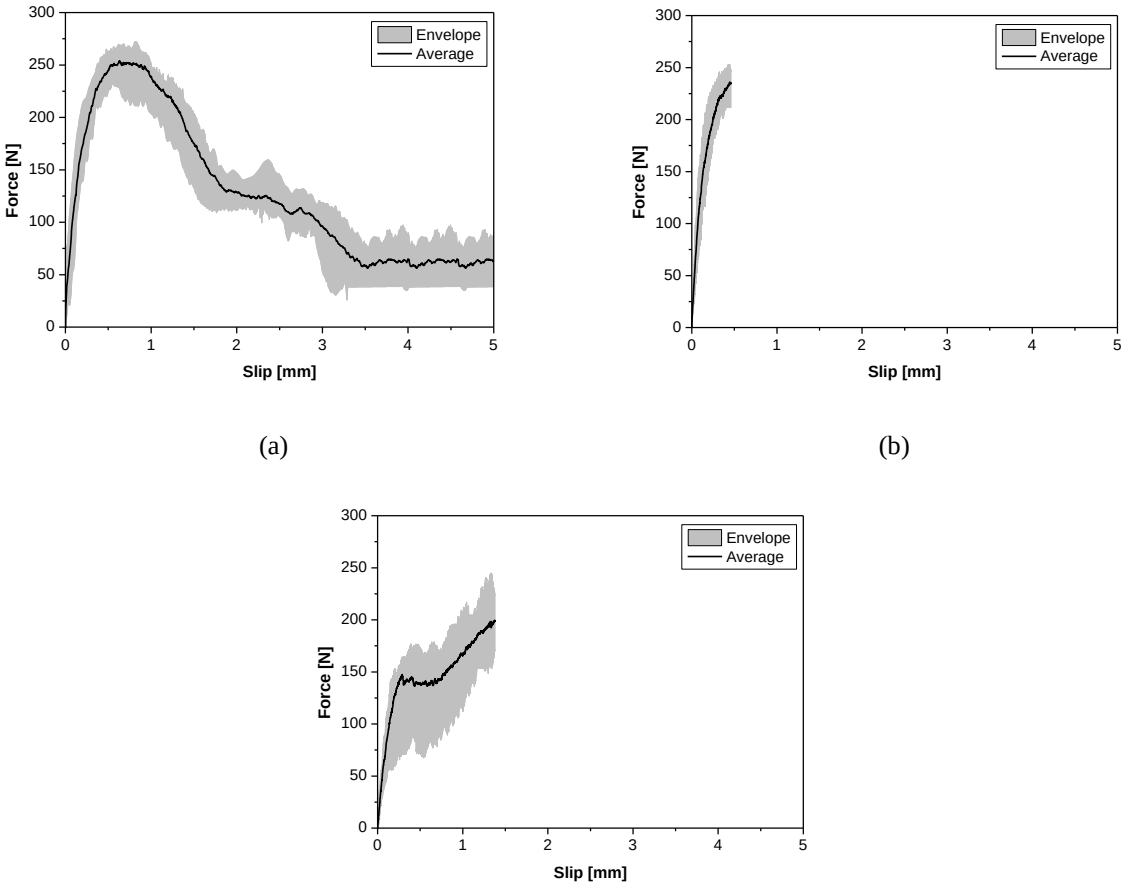

Fig. 8: Average monotonic pull-out load versus slip relationships for fibre inclination angles of: (a) 0°, (b) 30°and (c) 60°.

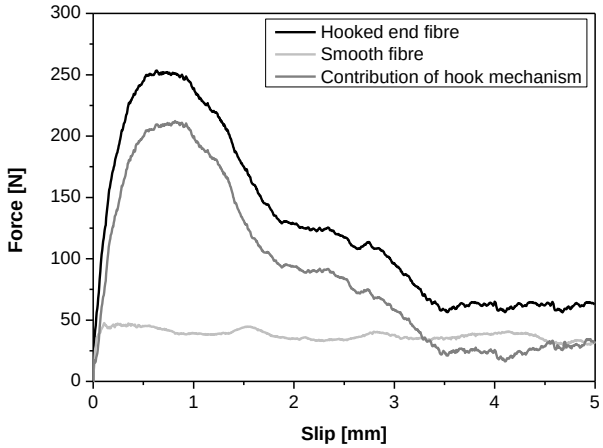

Fig. 9: Contribution of the end hook to the overall pull-out behaviour in fibres with inclination angle of 0°.

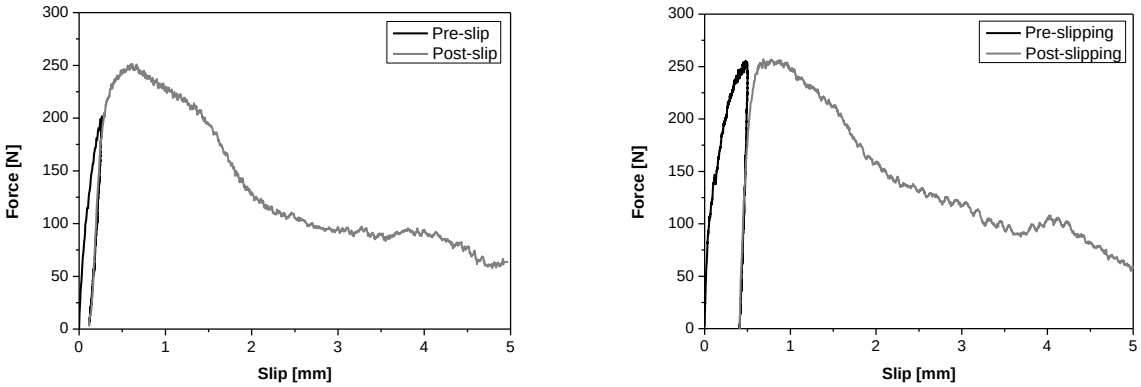

(a) (b)

Fig. 10: The average cyclic pull-out load – slip relationships for fibres with inclination angle of 0° and s_{pr} equals to: (a) 0.3 mm, and (b) 0.5 mm.

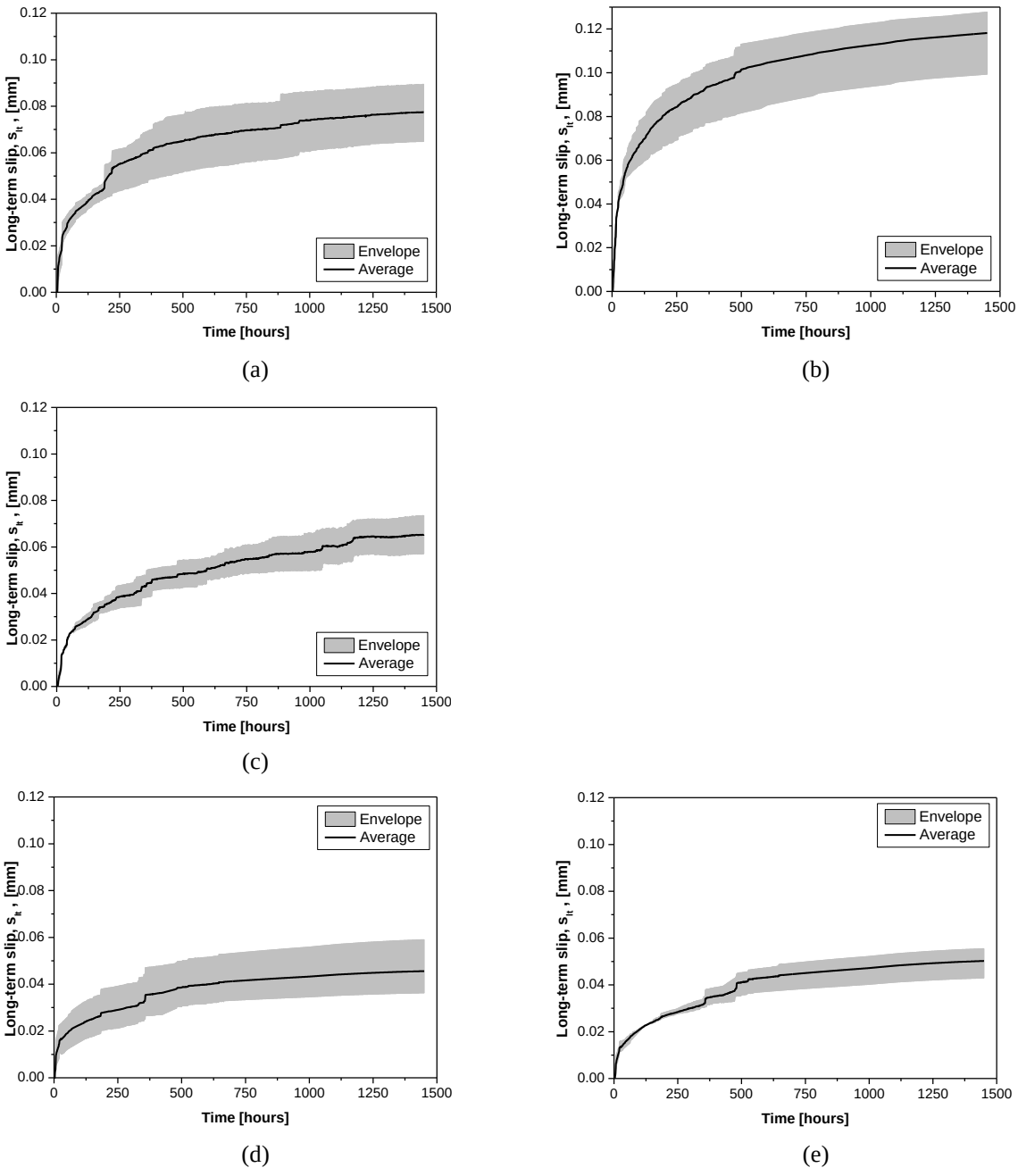

Fig. 11: Long-term slip versus time during fibre pull-out creep test: (a) and (b) 0 degree, (c) 30 degree, (d) and (e) 60 degree; (a), (c), (d) s_{pr} = 0.3 mm and (b), (e) s_{pr} = 0.5 mm.

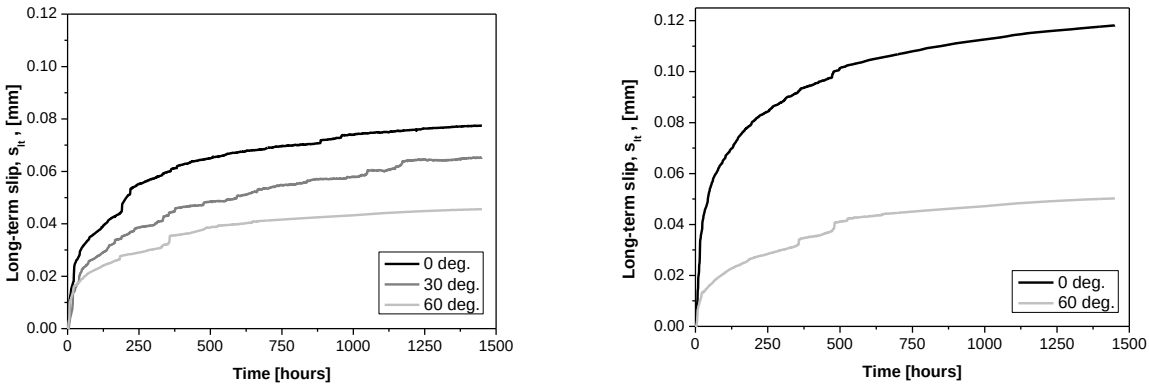

(a) (b)

Fig. 12: Long-term slip versus time for different fibre orientations and s_{pr} equal to: (a) 0.3 mm, and (b) 0.5 mm.

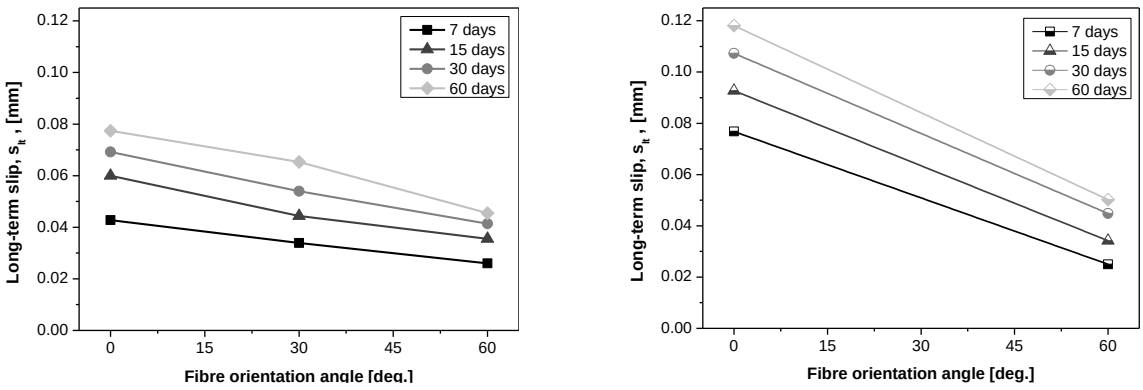

(a) (b)

Fig. 13: Influence of fibre orientation angle on the long-term slip for s_{pr} equal to: (a) 0.3 mm, and (b) 0.5 mm.

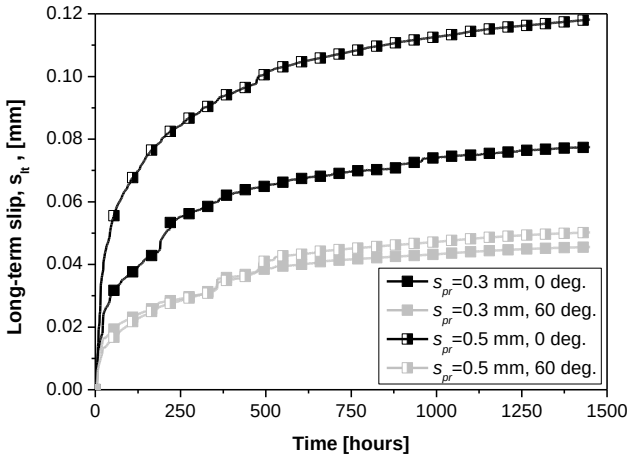

Fig. 14: Influence of pre-slip level on the development of long-term slip along time.

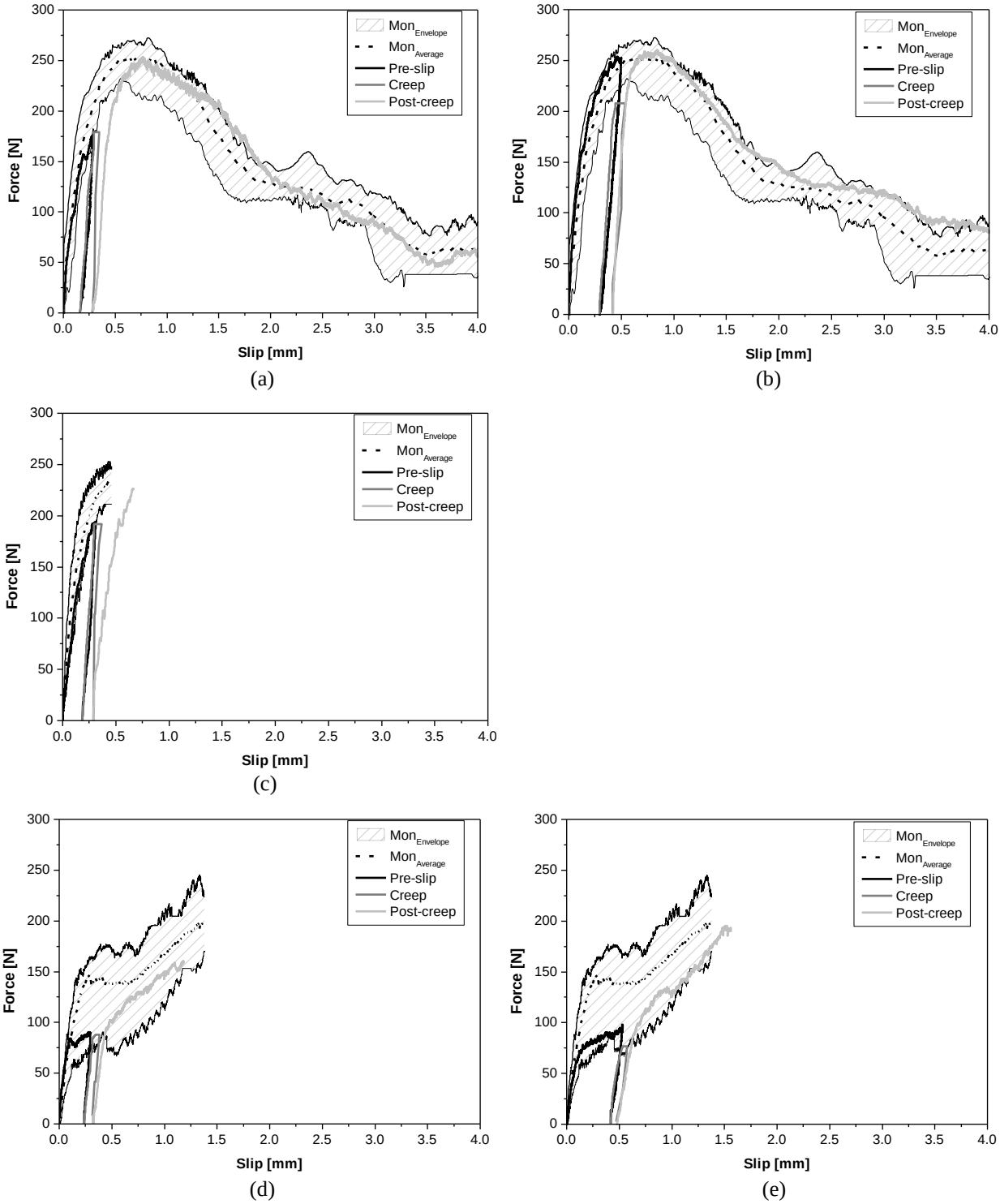

Fig. 15: Comparison of monotonic and long-term assembled curves: (a) and (b) 0 degree, (c) 30 degree, (d) and (e) 60 degree; (a), (c), (d)s_{pr} = 0.3 mm and (b), (e) s_{pr} = 0.5 mm.

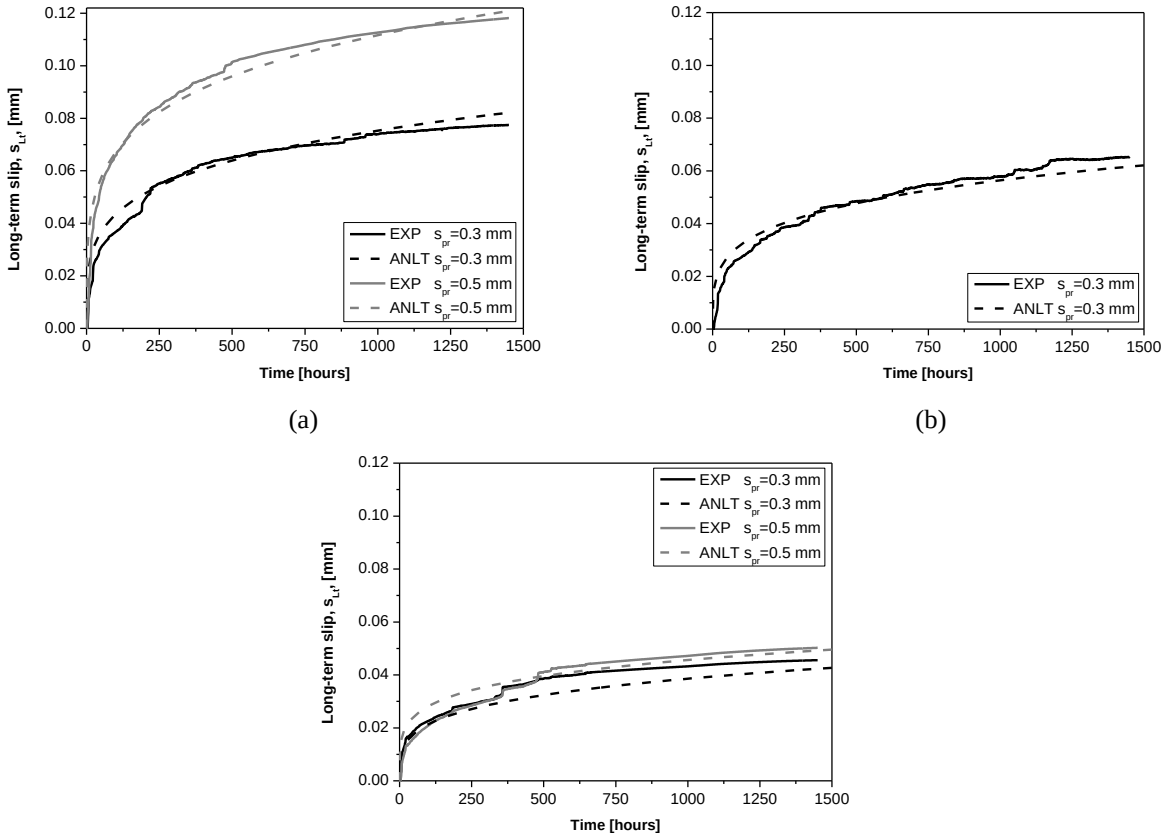

Fig. 16: Comparison between experimental and analytical long-term slip vs. time relationship for series with fibre inclination angle: (a) 0°, (b) 30° and (c) 60°.

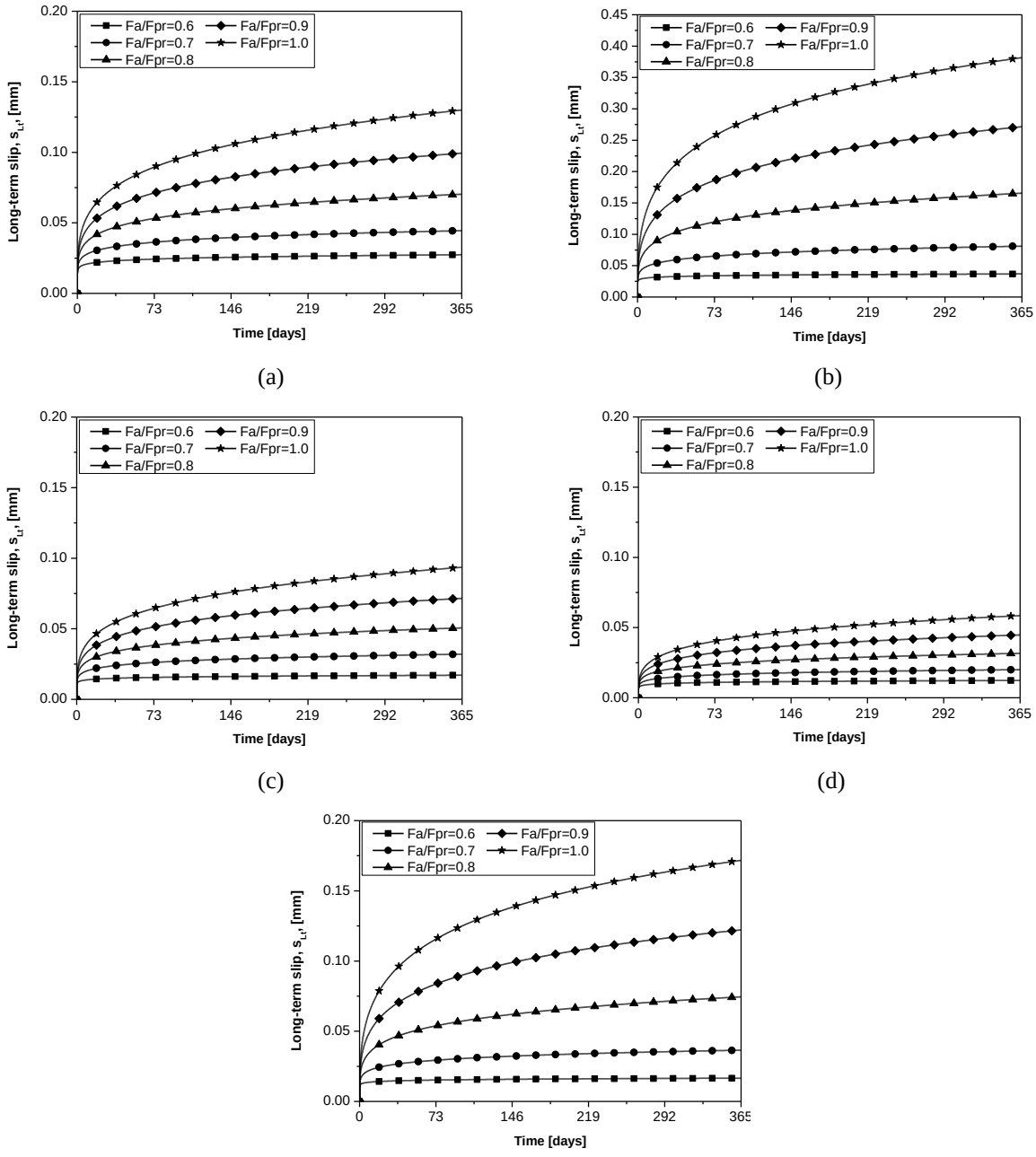

Fig. 17: Influence of F_a / F_{pr} on the long-term slip vs. time response for s_{pr} equal to: (a), (c), (d) 0.3 mm and (b), (e) 0.5 mm; fibre inclination angle of: (a), (b) 0° and (c) 30° and (d), (e) 60°.

Table 1: Mix constituents of self-compacting concrete per m^3.

Cement [kg]	Water [kg]	W/C [–]	SP [kg]	Lime stone filler [kg]	Fine sand [kg]	Coarse sand [kg]	Coarse aggregate [kg]
413	124	0.30	7.83	353	237	710	590

Table 2: Average slip rate for each pre-slip level (numbers in parenthesis represent CoV in %).

		Slip rate [μm/day]			
Pre-slip level	Orientation	7 days	15 days	30 days	60 days
0.3 mm	0	6.12 (8)	2.15 (34)	0.61 (23)	0.27 (16)
	30	7.15 (46)	1.75 (39)	0.63 (10)	0.22 (23)
	60	3.71 (32)	1.19 (23)	0.39 (14)	0.14 (31)
0.5 mm	0	10.97 (15)	1.99 (18)	0.97 (22)	0.36 (7)
	60	3.57 (6)	1.15 (32)	0.71 (26)	0.18 (11)

Table 3: Average creep coefficient at creep stage for each pre-slip level (numbers in parenthesis represent CoV in %).

		Creep coefficient at creep stage, φ^C, [-]			
Pre-slip level	Orientation	7 days	15 days	30 days	60 days
0.3 mm	0	0.259 (11)	0.358 (2)	0.412 (0.6)	0.463 (3)
	30	0.240 (9)	0.309 (10)	0.365 (11)	0.432 (19)
	60	0.198 (8)	0.269 (3)	0.352 (4)	0.394 (3)
0.5 mm	0	0.458 (0.4)	0.553 (2)	0.640 (4)	0.706 (4)
	60	0.230 (4)	0.317 (4)	0.373 (8)	0.410 (7)

Table 4: The average applied load in creep test (F_a, Fig. 5) and maximum load recorded during the pull-out test (F_{max}, Fig. 6) for each series of specimens.

	F_a (N)			F_{max} (N)		
s_{pr} (mm)	0°	30°	60°	0°	30°	60°
0.3	179	187	87	255	227	160
0.5	205	---	74	253	---	190